Convex approximations to the nonlinear AC Optimal Power Flow Problem

Waqquas Bukhsh

Abstract

This report documents several formulations of the optimal power flow problem (OPF) that are implemented as part of the Network Innovation Allowance project: *Application of convex optimisation to enhance National Grid's NOA process*. The code of formulations is made available on a GitHub repository [1]. The implemented models are tested on a 24-bus IEEE reliability test network and a 36-zone representative GB network. The results demonstrate that the convex approximation of the OPF problem can approximate the solution of the nonlinear OPF to good accuracy. Linear approximations to the OPF depends on the choice of initialisation and can only provide a good approximation if the initialisation is close to the optimal solution. The impact on voltages of committing a bank of capacitors is also demonstrated on the 36-zone network

Keywords

Convex analysis, power system analysis, optimal power flow problem, linear programming

Department of Electronic and Electrical Engineering, University of Strathclyde, United Kingdom
waqquas.bukhsh@strath.ac.uk

Contents

Nomenclature

Sets

$\mathscr{B}$ Buses, indexed by b.

$\mathscr{L}$ Lines, indexed by bb'.

$\mathscr{G}$ Generators, indexed by b.

$\mathscr{D}$ Loads, indexed by b.

$\mathscr{B}_b$ Buses connected to bus b.

$\mathscr{G}_b$ Generators located at bus b.

$\mathscr{D}_b$ Demands located at bus b.

Parameters

$G_b^{\mathrm{B}}, B_b^{\mathrm{B}}$ Shunt conductance, susceptance at bus b.

$g_{bb'}, b_{bb'}$ Conductance, susceptance of line bb'.

$b_{bb'}^{\mathrm{C}}$ Shunt susceptance of line bb'.

$\tau_{bb'}$ Off-nominal tap ratio of line bb'.

$V_b^{\mathrm{LB}}, V_b^{\mathrm{UB}}$ Min., max. voltage magnitude at bus b.

$P_g^{\mathrm{LB}}, P_g^{\mathrm{UB}}$ Min., max. real power outputs of generator g.

$Q_g^{\mathrm{LB}}, Q_g^{\mathrm{UB}}$ Min., max. reactive power outputs of generator g.

$P_d^{\mathrm{D}}, Q_d^{\mathrm{D}}$ Real, reactive power demands of load d.

S_l^+ Real power loss limit of line l.

$\Theta_{bb'}^+$ Max. angle across the line bb'.

$f_g(p_g^{\mathrm{G}})$ Generation cost function for generator g.

Variables

v_b, θ_b Voltage magnitude and phase at bus b.

$c_{bb'}$ $\cos\theta_{bb'}$. Note $c_{bb'} = c_{b'b}$.

$s_{bb'}$ $\sin\theta_{bb'}$. Note $s_{bb'} = -s_{b'b}$.

$p_g^{\mathrm{G}}, q_g^{\mathrm{G}}$ Real, reactive power outputs of generator g.

$p_d^{\mathrm{D}}, q_d^{\mathrm{D}}$ Real, reactive power supplied to load d.

Table 1. A list of optimisation models implemented in this project.

Model Name	Code Tag	Type	Capacitor/Reactor commitment	Suggested Solver
AC Optimal Power Flow	`ACOPF`	NLP	✗	`ipopt` [9]
Convex relaxation of ACOPF	`OPF_Convex`	QCP	✓	`cplex` [10]
Linearised ACOPF	`OPF_LP`	LP	✓	`cplex` [10]
PWL ACOPF	`OPF_PWL`	LP	✓	`cplex` [10]
DC OPF	`DCOPF`	LP	✓	`cplex` [10]

1. Introduction

The optimal power flow problem (OPF) is one of the most frequently and commonly solved optimisation problem in power systems analysis. The problem was first introduced by Carpentier [2] in 1962 and since then it has been used in numerous applications and has been extended in several ways to address questions in power systems [3, 4, 5]. The OPF problem is a nonlinear optimisation problem and there are two main issues involved in solving it. The first issue is the convergence of an OPF solution to an infeasible point and the second is the convergence to a local solution. Given the nonlinear nature of OPF, it is very challenging to overcome these two issues. The convergence of a solver to an infeasible point is usually detected by a solver, and feasibility might be restored by repeating the search from a different starting point. There are techniques in literature which aim to restore the feasibility of the OPF problem e.g. homotopy techniques to find a feasible solution for an OPF problem [6]. This is therefore not as serious problem as finding a local optimum without realising there is a better global solution.

This technical report provide details of several convex and linear approaches to solve the OPF problem. The advantage of convexifing or linearising the OPF problem is that it overcomes the issue of infeasibility and convergence to a local solution in the OPF problems. Table 1 presents the formulations that are discussed in this note. The code of these formulations is made available in a private[1] GitHub repository [1].

Each implementation of the OPF problem is classified as a nonlinear programming problem (NLP), quadratic convex programming (QCP) and linear programming problme (LP). This classification provides insights into the complexity of the problem. For example, linear problems are generally quicker to solver and always converge to a solution if the overall problem is feasible. However, the NLP problems are not guaranteed to converge even if the problem is feasible.

A solver is required to run the OPF models implemented in the code. A local installation of a solver is recommend, however, the code provides a way to access an online solver service NEOS [7] that can be used if a local installation of solver is not available. Table 1 provide two recommended solvers for solving the implemented formulations of the OPF problem. This is not an exhaustive list and other solvers could be used e.g. `gurobi` [8] instead of `cplex` and `ipopt`.

The rest of the technical note is arranged as follows. Section 2 presents the formulation of the nonlinear OPF problem in polar coordinates. A complete mathematical model the convex relaxation of the OPF is presented in Section 4.1. The proposed approach is tested on the IEEE 24-bus test case in Section 6. Finally, Section **??** provides a brief description of the future steps involved in the project,

2. The Optimal Power Flow Problem

This section presents a nonlinear mathematical formulation of the ACOPF problem. As noted earlier, the OPF problem is to minimise the cost of generation while supplying all the load and satisfying the bus voltage limits, the apparent power line limits and the real and reactive generator output power limits. The mathematical formulation in the polar coordinates is gives as follows:

[1] The private repository is not open-access. Contact waqquas.bukhsh@strath.ac.uk to gain access to the code

$$\min \sum_{g\in\mathcal{G}} f(p_g^{\mathrm{G}}) \tag{1a}$$

subject to

$$\sum_{g\in\mathcal{G}_b} p_g^{\mathrm{G}} = \sum_{d\in\mathcal{D}_b} P_d^{\mathrm{D}} + \sum_{b'\in\mathcal{B}_b} p_{bb'}^{\mathrm{L}} + G_b^{\mathrm{B}} u_b \tag{1b}$$

$$\sum_{g\in\mathcal{G}_b} q_g^{\mathrm{G}} = \sum_{d\in\mathcal{D}_b} Q_d^{\mathrm{D}} + \sum_{b'\in\mathcal{B}_b} q_{bb'}^{\mathrm{L}} - B_b^{\mathrm{B}} u_b \tag{1c}$$

$$p_{bb'}^{\mathrm{L}} = u_b G_{bb} + (G_{bb'} y_{bb'} + B_{bb'} z_{bb'}) \tag{1d}$$

$$q_{bb'}^{\mathrm{L}} = -u_b B_{bb} + (G_{bb'} z_{bb'} - B_{bb'} y_{bb'}) \tag{1e}$$

$$u_b = v_b^2 \tag{1f}$$

$$x_{bb'} = v_b v_{b'} \tag{1g}$$

$$y_{bb'} = x_{bb'} c_{bb'} \tag{1h}$$

$$z_{bb'} = x_{bb'} s_{bb'} \tag{1i}$$

$$c_{bb'} = \cos(\theta_b - \theta_{b'}) \tag{1j}$$

$$s_{bb'} = \sin(\theta_b - \theta_{b'}) \tag{1k}$$

$$\theta_{b_0} = 0 \tag{1l}$$

$$-\Theta_{bb'}^{+} \le \theta_b - \theta_{b'} \le \Theta_{bb'}^{+} \tag{1m}$$

$$V_b^{\mathrm{LB}} \le v_b \le V_b^{\mathrm{UB}} \tag{1n}$$

$$P_g^{\mathrm{LB}} \le p_g \le P_g^{\mathrm{UB}} \tag{1o}$$

$$Q_g^{\mathrm{LB}} \le q_g \le Q_g^{\mathrm{UB}} \tag{1p}$$

$$p_{bb'}^{\mathrm{L}\,2} + q_{bb'}^{\mathrm{L}\,2} \le (S_{bb'}^{\max})^2 \tag{1q}$$

where (1a) is the objective function, equations (1b)-(1c) are Kirchhoff's Current Law (KCL) enforcing active and reactive power balance, (1d)–(1e) are KVL, (1j)–(1k) are the trigonometric functions of angle difference across lines, (1l) removes the degeneracy in the bus voltage angles by fixing it to zero at the arbitrary reference bus, (1m) is the constraint on the angle difference, (1n)–(1p) are constraints on voltage and power generation, and (1q) are the line flow constraints. The line conductance $g_{bb'}$ and susceptance $b_{bb'}$ are defined by

$$g_{bb'} = \frac{r_{bb'}}{r_{bb'}^2 + x_{bb'}^2}, \qquad b_{bb'} = \frac{-x_{bb'}}{r_{bb'}^2 + x_{bb'}^2},$$

where $r_{bb'}$, $x_{bb'}$ are the line resistance and reactance, and parameters $G_{bb'}$ and $B_{bb'}$ are defined by

$$\begin{aligned}
&g_{bb'} = -\tau_{bb'} G_{bb'} = -\tau_{bb'} G_{b'b} = G_{b'b'} = \tau_{bb'}^2 G_{bb}, \\
&b_{bb'} + 0.5 b_{bb'}^{\mathrm{C}} = B_{b'b'} = \tau_{bb'}^2 B_{bb}, \\
&-b_{bb'} = \tau_{bb'} B_{b'b} = \tau_{bb'} B_{bb'},
\end{aligned}$$

where $b_{bb'}^{\mathrm{C}}$ is the line charging susceptance and $\tau_{bb'} = 1$ except in transformer "lines", where it is the tap ratio and (as in the MATPOWER [11] convention) the ideal transformer is at the b end of the line. This formulation os OPF is nonconvex and in [12] test cases are reported with local solutions of OPF.

3. Nonlinearities in the ACOPF problem

Equations 1 presented the nonlinear ACOPF formulation. We note that the nonlinearities are present in equations (1f - 1k), (1q).

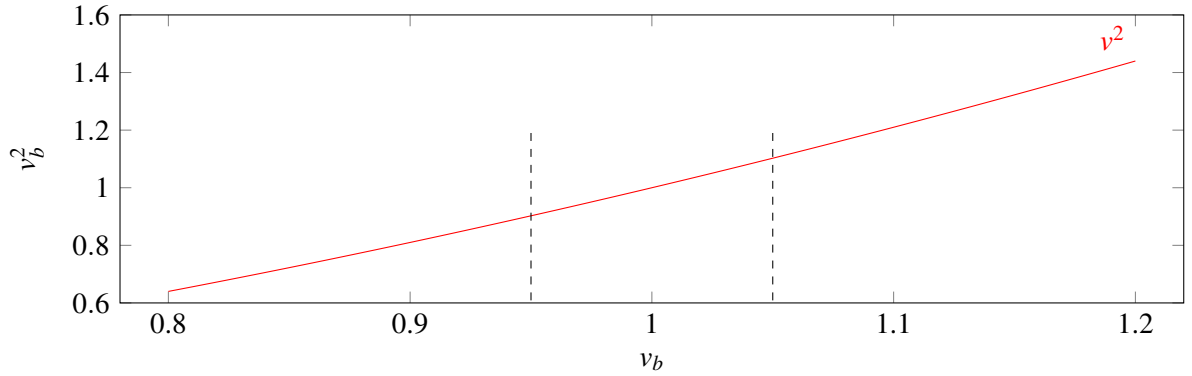

Figure 1. Voltage squared for ±20% of the nominal voltage. Dashed lines are the operational voltage bounds from the SQSS [13]

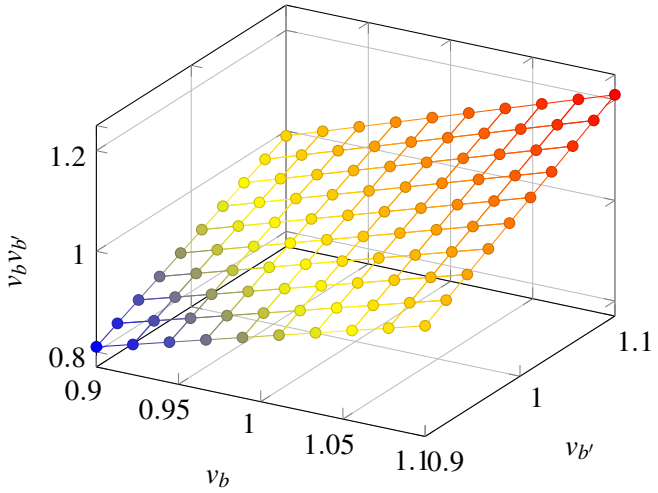

Figure 2. Bilinear function of voltages at either end of a line.

3.1 Voltage squared

The voltage squared term is a nonlinear function and it appears in the power balance equations (1b,1c) and the power flow equations (1d,1e). In the nonlinear ACOPF, we have denoted the voltage square at a bus b by the variable u_b.

Figure 1 presents the graph of voltage squared term within ±20% of the nominal value of a voltage at a bus b. The dashed lines presents the SQSS operational bounds on the voltage magnitude which are ±5% of the nominal value. We observe that within these bounds the voltage squared term can be approximated quite accurately with a linear function.

3.2 Binlinear term

Equation (1g) is a nonlinear function that is defined by the product of voltage magnitudes at either end of a line connection two buses b and b', respectively. Figure 2 presents a graph of the bilinear function for voltage ranges of ±10%. We observe that the surface of the bilinear function can be approximated by a plane with good accuracy.

3.3 Sine function

The nonlinear sine function appears in the power flow equations. Figure 3 presents the graph of a sine function for an angle differences between −60 and 60 degrees. We note that the sine function can be approximated by a linear function when the angle differences are small. However, as the angle differences increase the curvature of the sine function increases.

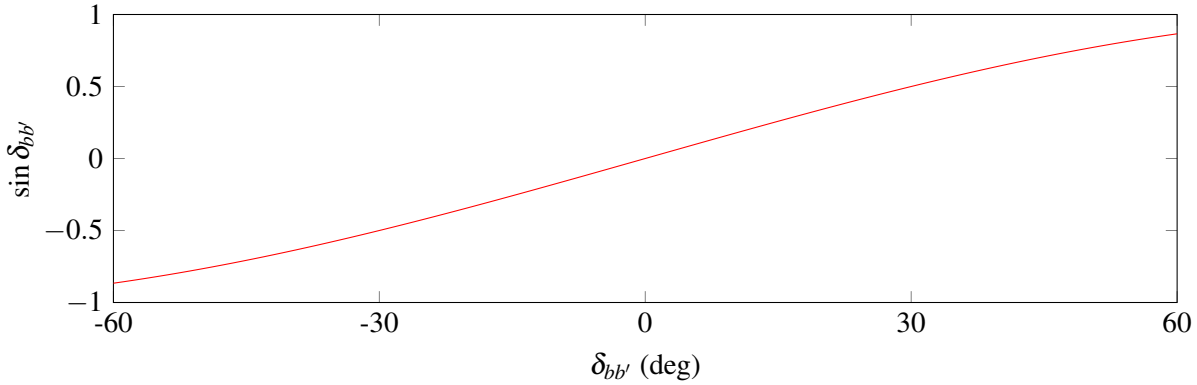

Figure 3. Sine function.

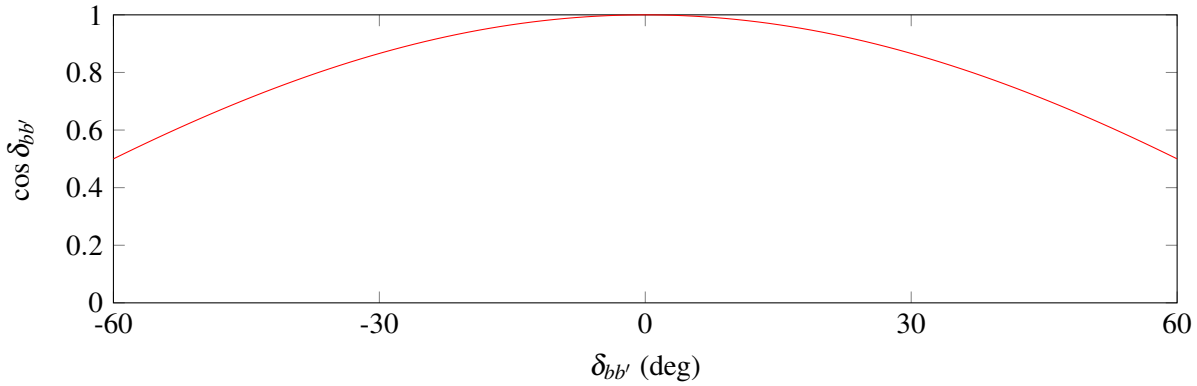

Figure 4. Cosine function.

3.4 Cosine function

Figure 4 presents the graph of the cosine function. This is a tricky function to approximation with a linear function as the rate of change of this function changes sign at 0.

3.5 Product of trigonometric and bilinear functions

In the previous subsections, we discussed the individual nonlinear functions that are presents in the OPF formulation. The power flow equations involve product of these nonlinear functions i.e. Equations (1h,1i). These bilinear equations in the new variables again needs to be linearised (or convexified) which not only adds to the complexity of the overall approximation but also introduces approximation errors. The next section provides a step wise approach to several convex and linear approximations of the OPF problem.

4. Convex and linear approximations of the ACOPF

4.1 A convex approximation of the ACOPF problem

This section presents a convex relaxation of the problem defined in Equations 1. The approach presented here is motivated by the work of [14].

4.1.1 Convex Envelopes for quadratic terms

Let V_b^{LB}, V_b^{UB} be the lower and upper bound of the voltage at bus b. The relaxation of quadratic term is given by the following two inequalities:

$$v_b^2 \leq u_b, \tag{2a}$$

$$u_b \leq (V_b^{\mathrm{LB}} + V_b^{\mathrm{UB}})v_b - V_b^{\mathrm{LB}} V_b^{\mathrm{UB}}. \tag{2b}$$

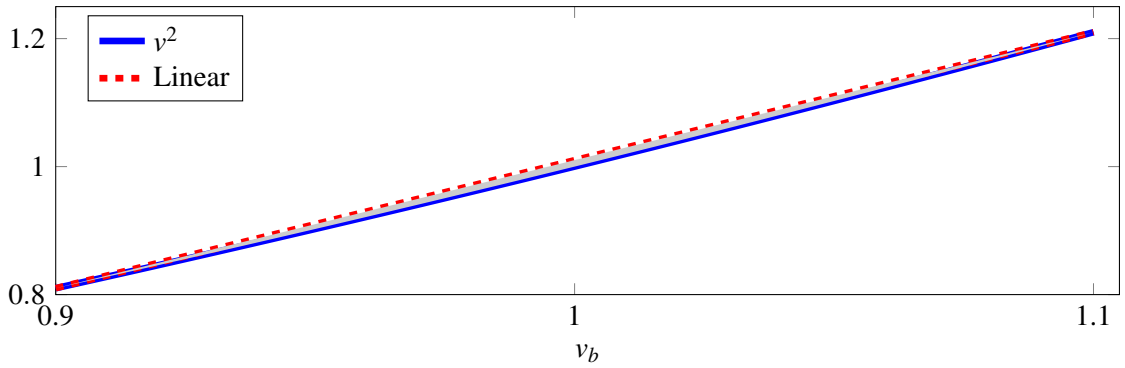

Figure 5. Convex envelopes of the voltage square term.

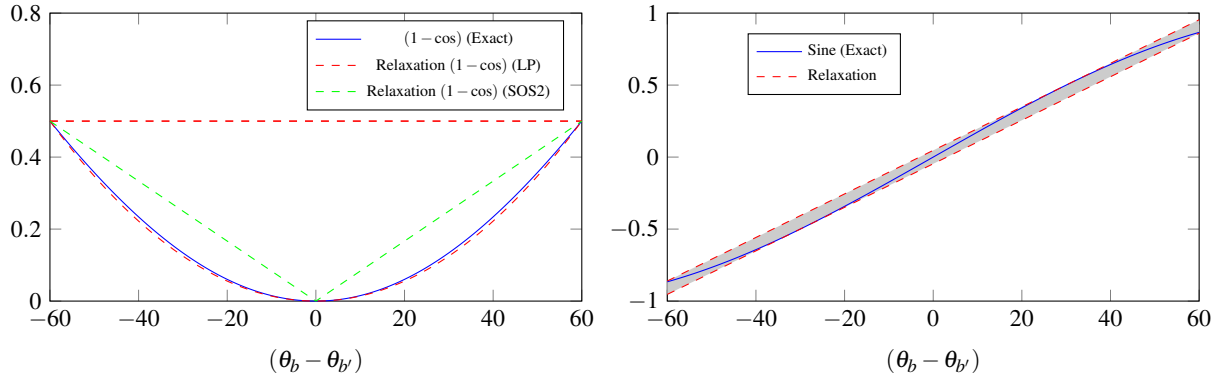

(a) Quadratic relaxation of 1-cosine function. **(b)** Quadratic relaxation of sine function.

Figure 6. Convex relaxation of trigonometric functions.

The inequalities in (2a-2b) are convex and linear respectively. The feasible region defined by the two inequalities for $\pm 10\%$ voltage bounds is shown in gray in Fig. 5. For this case the maximum error of 0.01p.u. in the approximation of (2) occurs at 1 p.u.

4.1.2 Relaxation of Bilinear Terms

The bilinear functions can be approximated linearly using McCormick inequalities [15]. These inequalities bound the bilinear function using linear planes. The linear approximation of Equations 1g is provided as follows:

$$x_{bb'} \geq V_b^{\mathrm{LB}} v_{b'} + V_{b'}^{\mathrm{LB}} v_b - V_b^{\mathrm{LB}} V_{b'}^{\mathrm{LB}}, \tag{3a}$$
$$x_{bb'} \geq V_b^{\mathrm{UB}} v_{b'} + V_{b'}^{\mathrm{UB}} v_b - V_b^{\mathrm{UB}} V_{b'}^{\mathrm{UB}}, \tag{3b}$$
$$x_{bb'} \leq V_b^{\mathrm{LB}} v_{b'} + V_{b'}^{\mathrm{UB}} v_b - V_b^{\mathrm{LB}} V_{b'}^{\mathrm{UB}}, \tag{3c}$$
$$x_{bb'} \leq V_b^{\mathrm{UB}} v_{b'} + V_{b'}^{\mathrm{LB}} v_b - V_b^{\mathrm{UB}} V_{b'}^{\mathrm{LB}}. \tag{3d}$$

The above four inequalities forms a vertex polyhedral enclosing the bilinear function $v_b v_{b'}$. For the voltage bounds of $\pm 10\%$ of the 1 p.u., and the bilinear function is quite flat in this region and the maximum error in the approximation using McCormick inequalities is 0.01 p.u. and it occurs at 1 p.u.

4.1.3 Quadratic Relaxation of cosine function

A quadratic relaxation of $c_{bb'}$ defined in Equation 1j is given as follows:

$$c_{bb'} = \frac{\cos(\Theta^+_{bb'})}{(\Theta^+_{bb'})^2}\phi_{bb'}, \tag{4a}$$
$$(\theta_b - \theta_{b'})^2 \leq \phi_{bb'}, \tag{4b}$$
$$\phi_{bb'} \leq (\Theta^+_{bb'})^2. \tag{4c}$$

Note that here we have used $\phi_{bb'} \sim (\theta_b - \theta_{b'})^2$. Fig. 6a shows the quadratic relaxation of $(1-\cos)$ function over the interval $[-60^\circ, 60^\circ]$. The relaxation evaluates exactly on 0°, and at the end points.

The real power lost in a line bb' is proportional to $1 - cos(\theta_b - \theta_{b'})$. So we expect that the objective of OPF to push towards the interior of this function. However it is generally not true, especially in the cases where global solution has high line losses. In these cases this approximation will perform poorly because of the error introduced by the constraint 4c. An alternate way of approximating cosine function is to use special ordered sets of type 2 (SOS2) [16]. To do this we introduced an order set of variable weights $\{\alpha^-_{bb'}, \alpha^0_{bb'}, \alpha^+_{bb'}\}$ and replace the inequality in (4c) with the following:

$$\phi_{bb'} \leq -\alpha^-_{bb'}\Theta^+_{bb'} + \alpha^+_{bb'}\Theta^+_{bb'} \tag{5a}$$
$$\alpha^-_{bb'} + \alpha^0_{bb'} + \alpha^+_{bb'} = 1, \tag{5b}$$
$$0 \leq \alpha^-_{bb'}, \alpha^0_{bb'}, \alpha^+_{bb'} \leq 1. \tag{5c}$$

The green dashed line in Fig. 6a shows the improvement using SOS2 formulation. Now we provide two approximations of $y_{bb'}$ as follows:

Approximation 1 Let $X^{\text{LB}}_{bb'}$, $X^{\text{UB}}_{bb'}$ be the lower and upper bound of $x_{bb'}$, respectively. Also let $C^{\text{LB}}_{bb'}$, $C^{\text{UB}}_{bb'}$ be the lower and upper bound of $c_{bb'}$. Following inequalities gives the approximation of $y_{bb'}$:

$$y_{bb'} \geq X^{\text{LB}}_{bb'}c_{bb'} + C^{\text{LB}}_{bb'}x_{bb'} - X^{\text{LB}}_{bb'}C^{\text{LB}}_{bb'}, \tag{6a}$$
$$y_{bb'} \geq X^{\text{UB}}_{bb'}c_{bb'} + C^{\text{UB}}_{bb'}x_{bb'} - X^{\text{UB}}_{bb'}C^{\text{UB}}_{bb'}, \tag{6b}$$
$$y_{bb'} \leq X^{\text{LB}}_{bb'}c_{bb'} + C^{\text{UB}}_{b'}x_{bb} - X^{\text{LB}}_{bb'}C^{\text{UB}}_{bb'}, \tag{6c}$$
$$y_{bb'} \leq X^{\text{UB}}_{bb'}c_{bb'} + C^{\text{LB}}_{bb'}x_{bb'} - X^{\text{UB}}_{bb'}C^{\text{LB}}_{bb'}. \tag{6d}$$

Approximation 2 In [14], the approximation of $y_{bb'}$ is done by the following set of constraints:

$$y_{bb'} = \left(\frac{1-\cos(\Theta^+_{bb'})}{(\Theta^+_{bb'})^2}\right) V^{\text{LB}}_b V^{\text{LB}}_{b'}\phi_{bb'}, \tag{7a}$$
$$(\theta_b - \theta_{b'})^2 \leq \phi_{bb'}, \tag{7b}$$
$$\phi_{bb'} \leq (\Theta^+_{bb'})^2. \tag{7c}$$

Note that in this approximation the nonlinear term $v_b v_{b'}$ is not approximated by the McCormick inequalities. Numerical tests shows that the objective function change upto 1% by modelling the bilinear function using McCormick inequalities.

4.1.4 Convex Relaxation of sine function

Let $S^{\mathrm{LB}}_{bb'}$, $S^{\mathrm{UB}}_{bb'}$ be the lower and upper bound of the sine function. The polyhedral envelope of sine function (see Fig. 6B) is given by the following two inequalities:

$$s_{bb'} \leq \cos\left(\frac{\Theta^{+}_{bb'}}{2}\right)\left(\theta_b - \theta_{b'} - \frac{\Theta^{+}_{bb'}}{2}\right) + \sin\left(\frac{\Theta^{+}_{bb'}}{2}\right), \tag{8a}$$

$$s_{bb'} \geq \cos\left(\frac{\Theta^{+}_{bb'}}{2}\right)\left(\theta_b - \theta_{b'} + \frac{\Theta^{+}_{bb'}}{2}\right) - \sin\left(\frac{\Theta^{+}_{bb'}}{2}\right). \tag{8b}$$

The bilinear function $z_{bb'}$ can be approximated by the McCormick inequalities as:

$$x_{bb'} \geq S^{\mathrm{LB}}_{bb'}u_{bb'} + X^{\mathrm{LB}}_{bb'}s_{bb'} - S^{\mathrm{LB}}_{bb'}X^{\mathrm{LB}}_{bb'}, \tag{9a}$$

$$x_{bb'} \geq S^{\mathrm{UB}}_{bb'}u_{bb'} + X^{\mathrm{UB}}_{bb'}s_{bb'} - S^{\mathrm{UB}}_{bb'}X^{\mathrm{UB}}_{bb'}, \tag{9b}$$

$$x_{bb'} \leq S^{\mathrm{LB}}_{bb'}u_{bb'} + X^{\mathrm{UB}}_{bb'}s_{bb'} - S^{\mathrm{LB}}_{bb'}X^{\mathrm{UB}}_{bb'}, \tag{9c}$$

$$x_{bb'} \leq S^{\mathrm{UB}}_{bb'}u_{bb'} + X^{\mathrm{LB}}_{bb'}s_{bb'} - S^{\mathrm{UB}}_{bb'}X^{\mathrm{LB}}_{bb'}, \tag{9d}$$

where $S^{\mathrm{LB}}_{bb'} = -\sin(\Theta^{+}_{bb'})$, $S^{\mathrm{UB}}_{bb'} = \sin(\Theta^{+}_{bb'})$, $U^{\mathrm{LB}}_{bb'} = V^{\mathrm{LB}}_{b}V^{\mathrm{LB}}_{b'}$, $U^{\mathrm{UB}}_{bb'} = V^{\mathrm{UB}}_{b}V^{\mathrm{UB}}_{b'}$.

4.1.5 Overall formulation of the OPF as a QCP

We replace the nonconvex constraints in Equations 1 by their linear/convex counterparts to obtain a quadratic convex programming problem (QCP). The overall formulation is as follows:

$$\min \sum_{g\in\mathscr{G}} f(p^{\mathrm{G}}_g), \tag{10a}$$

subject to

$$\sum_{g\in\mathscr{G}_b} p^{\mathrm{G}}_g = \sum_{d\in\mathscr{D}_b} P^{\mathrm{D}}_d + \sum_{b'\in\mathscr{B}_b} p^{\mathrm{L}}_{bb'} + G^{\mathrm{B}}_b t_b, \tag{10b}$$

$$\sum_{g\in\mathscr{G}_b} q^{\mathrm{G}}_g = \sum_{d\in\mathscr{D}_b} Q^{\mathrm{D}}_d + \sum_{b'\in\mathscr{B}_b} q^{\mathrm{L}}_{bb'} - B^{\mathrm{B}}_b t_b, \tag{10c}$$

$$(3-6), (8-10), \tag{10d}$$

$$\theta_{b_0} = 0, \tag{10e}$$

$$-\Theta^{+}_{bb'} \leq \theta_b - \theta_{b'} \leq \Theta^{+}_{bb'}, \tag{10f}$$

$$V^{\mathrm{LB}}_b \leq v_b \leq V^{\mathrm{UB}}_b, \tag{10g}$$

$$P^{\mathrm{LB}}_g \leq p_g \leq P^{\mathrm{UB}}_g, \tag{10h}$$

$$Q^{\mathrm{LB}}_g \leq q_g \leq Q^{\mathrm{UB}}_g, \tag{10i}$$

$$p^{\mathrm{L}}_{bb'}{}^2 + q^{\mathrm{L}}_{bb'}{}^2 \leq (S^{\max}_{bb'})^2. \tag{10j}$$

4.2 Strengthening Convex relaxation of optimal power flow with redundant constraints

The real and reactive power lost in a line can be obtained by adding the real and reactive power flows from either ends of the line respectively:

$$p^{\mathrm{L}}_{bb'} + p^{\mathrm{L}}_{b'b} = v_b^2 G_{bb} + v_{b'}^2 G_{b'b'} + 2v_b v_{b'} G_{bb'} c_{bb'}, \tag{11a}$$

$$q^{\mathrm{L}}_{bb'} + q^{\mathrm{L}}_{b'b} = -v_b^2 B_{bb} - v_{b'}^2 B_{b'b'} - 2v_b v_{b'} B_{bb'} c_{bb'}. \tag{11b}$$

Using the convex relaxation of nonlinearities, we can write Eqs. (11) in the following form:

$$p^{\mathrm{L}}_{bb'} + p^{\mathrm{L}}_{b'b} = t_b G_{bb} + t_{b'} G_{b'b'} + 2G_{bb'}(u_{bb'} - w_{bb'}), \tag{12a}$$
$$q^{\mathrm{L}}_{bb'} + q^{\mathrm{L}}_{b'b} = -t_b B_{bb} - t_{b'} B_{b'b'} - 2B_{bb'}(u_{bb'} - w_{bb'}), \tag{12b}$$

but numerical tests show that including the Eqs. (12) in the formulation does not make any difference. Another way of writing the loss in a transmission line is:

$$p^{\mathrm{L}}_{bb'} + p^{\mathrm{L}}_{b'b} = g_{bb'}\left((\hat{v}_b - v_{b'})^2 + 2w_{bb'}\right), \tag{13a}$$
$$q^{\mathrm{L}}_{bb'} + q^{\mathrm{L}}_{b'b} = -b_{bb'}\left((\hat{v}_b - v_{b'})^2 + 2w_{bb'}\right), \tag{13b}$$

where $\hat{v}_b = \frac{v_b}{\tau_{bb'}}$. Let $d_{bb'} \sim (\tilde{v}_b - v_{b'})^2$. The convex relaxation of (13) can be written as:

$$p^{\mathrm{L}}_{bb'} + p^{\mathrm{L}}_{b'b} = g_{bb'}\left(d_{bb'} + 2w_{bb'}\right), \tag{14a}$$
$$q^{\mathrm{L}}_{bb'} + q^{\mathrm{L}}_{b'b} = -b_{bb'}\left(d_{bb'} + 2w_{bb'}\right), \tag{14b}$$
$$(\hat{v}_b - v_{b'})^2 \leq d_{bb'}, \tag{14c}$$
$$d_{bb'} \leq (D^{\mathrm{LB}} + D^{\mathrm{UB}})(\tilde{v}_b - v_{b'}) - D^{\mathrm{LB}} D^{\mathrm{UB}}, \tag{14d}$$

where $D^{\mathrm{LB}} = \frac{V_b^{\mathrm{LB}}}{\tau_{bb'}} - V_{b'}^{\mathrm{UB}}$ and $D^{\mathrm{UB}} = \frac{V_b^{\mathrm{UB}}}{\tau_{bb'}} - V_{b'}^{\mathrm{LB}}$.

Authors in [14] reported that including constraints (14) in the convex relaxation of OPF the gap can be improved by 90% in some cases.

4.3 A linear approximation of the ACOPF problem

In this subsection, a linear approximation of the ACOPF problem is provide that is build using first order Taylor series approximation. A Taylor series approximation of a function with three variables is given as follows:

$$f(x,y,z) \approx f(x_0,y_0,z_0) + (x - x_0)\frac{\partial f}{\partial x} + (y - y_0)\frac{\partial f}{\partial y} + (z - z_0)\frac{\partial f}{\partial z} \tag{15}$$

where (x_0, y_0, z_0) is a point where the linear approximation is based. We note that the accuracy of the Taylor series approximation depends on point of linearisation.

Table 2 presents a comparison of nonlinear and linearised function evaluations of the nonlinear functions that appear in the ACOPF formulation. We note that the LP approximation is exact at the point of linearisation (first row in the table). However, as we move away from the point of linearisation the accuracy of the linearisation deteriorates (second and third row in the table).

4.4 A piecewise linear approximation of the ACOPF problem

As noted earlier in this report, cosine function is a particularly challenging function to approximate because of it's curvature. A linear approximation of cosine is poor. This section propose a formulation that using piecewise linear approximation of the cosine function.

Figure 7 presents a piecewise linear approximation of the cosine function using two and four sections, respectively. We note that the accuracy of the approximation improves with increasing number of sections. The number of section is a parameter in the code that a user can choose.

The n-sections in piecewise linear approximation of the cosine function are created by equidistant (n+1) points on the x-axis. An alternate approach is to dynamically choose the (n+1) points such that the points are closer near to the origin (where the curvature of the cosine function is greater) and less at the edges where curvature is small. Figure 8 presents a dynamic selection of the points on the x-axis. This can be achieved by the providing an error estimate ε in the code that automatically creates a set of points on the x-axis such that the piecewise linear approximation error is always less than the *epsilon*.

Table 2. Comparison of function values of nonlinear and LP approximation

	Function	Function Value	LP Approximation ($v_1 = v_2 = 1, \delta_{12} = 0$)
$v_1 = v_2 = 1.00, \delta_{12} = 0$	v_1^2	1.0000	1.0000
	$v_1 v_2 \sin(\delta_{12})$	0.0000	0.0000
	$v_1 v_2 \cos(\delta_{12})$	1.0000	1.0000
$v_1 = v_2 = 0.95, \delta_{12} = 15^\circ$	v_1^2	0.9025	0.9000
	$v_1 v_2 \sin(\delta_{12})$	0.2336	0.2618
	$v_1 v_2 \cos(\delta_{12})$	0.8717	0.9000
$v_1 = v_2 = 1.05, \delta_{12} = 30^\circ$	v_1^2	1.1025	1.1000
	$v_1 v_2 \sin(\delta_{12})$	0.5512	0.5236
	$v_1 v_2 \cos(\delta_{12})$	0.9548	1.1000

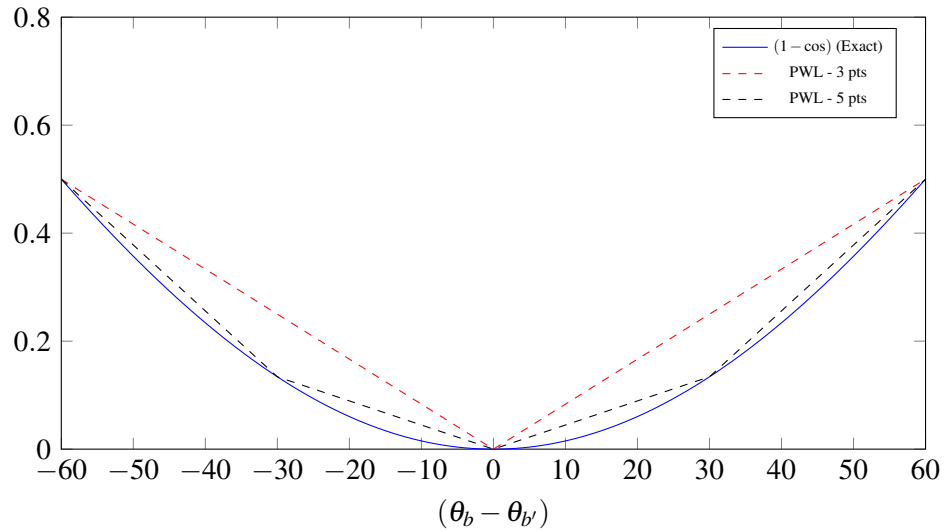

Figure 7. Piecewise linearization of the cosine function

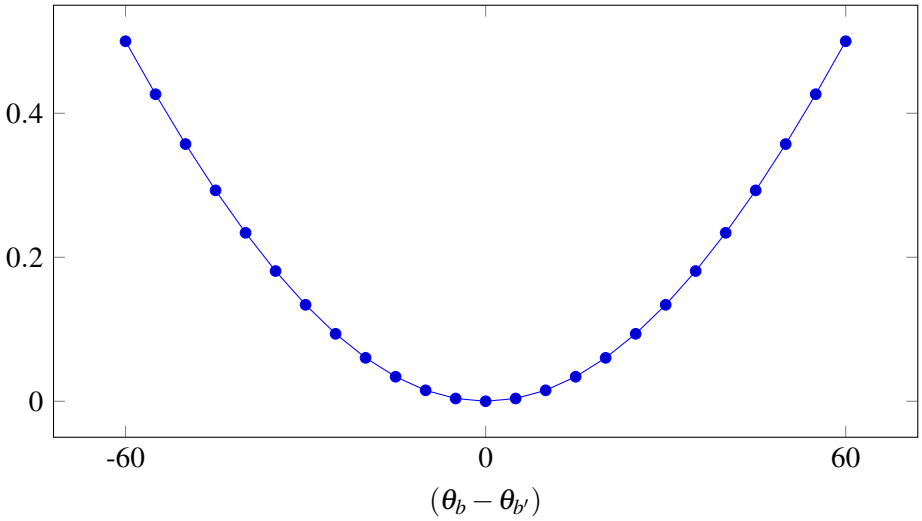

Figure 8. Dynamic piecewise linearisation of the cosine function

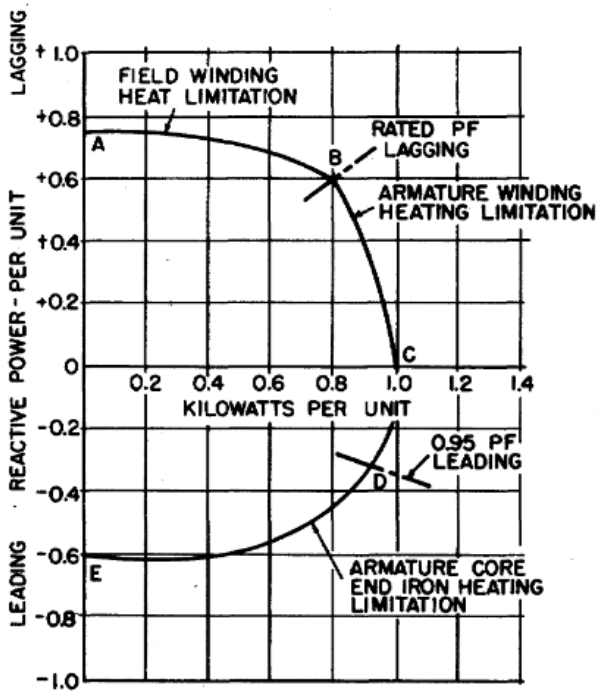

(a) A typical generator's capability curve [17]

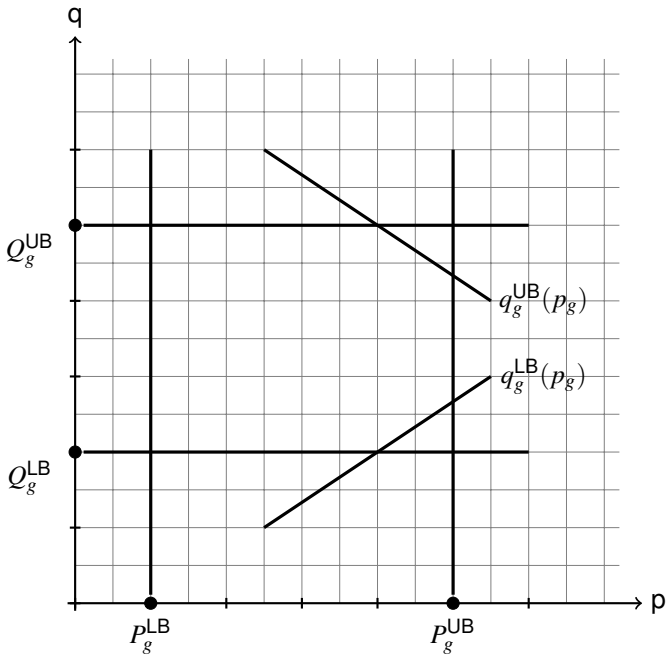

(b) Modelling of generator capability using piecewise function of Q-limits.

Figure 9. A typical generator's capability curve, also known as 'D-curve' can be approximated using linear cuts to the standard rectangular feasible region defined by the active and reactive power constraints. The exact definition of these linear cuts depends on individual generating units.

5. Modelling of Electrical Components

5.1 Modelling of Generator Capability Curves

In most OPF implementations, the active and reactive power generator outputs are modelled independently using the following constraints:

$$P_g^{\mathrm{LB}} \leq p_g \leq P_g^{\mathrm{UB}} \tag{16a}$$
$$Q_g^{\mathrm{LB}} \leq q_g \leq Q_g^{\mathrm{UB}} \tag{16b}$$

This is an approximation and a detailed model is required to accurately characterise generator capability curves, which are also known as 'D-curves'. A typical generator capability curve is presented in Figure 9(a) and an approximation of it using linear constraints is presented in Figure 9(b).

$$P_g^{\mathrm{LB}} \leq p_g \leq P_g^{\mathrm{UB}} \tag{17a}$$
$$q_g^{\mathrm{LB}}(p_g) \leq q_g \leq q_g^{\mathrm{UB}}(p_g) \tag{17b}$$

5.2 Modelling of the SVCs

Static Var Compensators (SVC) is a type of shunt FACT devices, which react to a system's conditions and provide reactive power support to minimise system losses and maintain a steady voltage profile. The installation of SVCs in a system has the potential of increasing a system active power transfer capabilities while meeting voltage constraints.

In an optimal power flow problem, an SVC can be modelled as a generator using the following constraint:

$$0 \leq p_g \leq 0 \tag{18a}$$
$$Q^{\min} \leq q_g \leq Q^{\max} \tag{18b}$$

Note that an SVC can be capacitive or inductive within a range specified by it's bounds [18].

5.3 Commitment of capacitors/reactors

The capacitor banks and reactors can be switched in or out of the system depending on the operational conditions. Let η_b^{ind}, η_b^{cap} be binary variables that models the commitment of capacitor and a reactor at bus b, respectively. Their commitment can be modelled using the following expression on the RHS of the Equation 1c.

$$\left(-B^{\text{ind}}\eta_b^{\text{ind}} + B^{\text{cap}}\eta_b^{\text{cap}}\right) v_b^2 \tag{19}$$

Note that the above equation is nonlinear as it involved product of a binary variable with voltage square. Instead of using the above nonlinear expression, we use the following linear inequalities

$$Q_b^{\text{Min}}(1-\eta_b^{\text{ind}}) - B^{\text{ind}}u_b \leq q_b^{\text{ind}} \leq (1-\eta_b^{\text{ind}})Q_b^{\text{Max}} \tag{20a}$$
$$Q_b^{\text{Min}}\eta_b^{\text{ind}} \leq q_b^{\text{ind}} \leq \eta_b^{\text{ind}}Q_b^{\text{Max}} \tag{20b}$$
$$Q_b^{\text{Min}}(1-\eta_b^{\text{cap}}) - B^{\text{cap}}u_b \leq q_b^{\text{cap}} \leq (1-\eta_b^{\text{cap}})Q_b^{\text{Max}} \tag{20c}$$
$$Q_b^{\text{Min}}\eta_b^{\text{cap}} \leq q_b^{\text{cap}} \leq \eta_b^{\text{cap}}Q_b^{\text{Max}} \tag{20d}$$

where $q_b^{\text{ind}}, q_b^{\text{cap}}$ are the inductance and conductive contribution of the committed reactors and capacitors, respectively.

6. Demonstration

Figure 10(a) presents the single line diagram of the 24-bus IEEE reliability test network. The test network consists of 24 buses, 33 generators and 33 branches. There are 5 transformers which connect the two 138 kV and 230 kV voltage areas. Figure 10(b) presents a 400 kV representative GB network with 36 zones, 96 generators and 66 lines.

Figure 11 presents voltage profile of results obtained by the models ACOPF and convex OPF, respectively. Figure 11(a) is the voltage profile when both the models run without any voltage targets and the optimisation is free to choose voltages at the buses in a network. We observe that the convex solution always underestimate the voltage magnitude at the buses. And since the convex model is a relaxation it also underestimates the cost of meeting demand i.e. it can meet demand at lower losses than the nonlinear ACOPF. Figure 11(b) presents the voltage profile when the convex ACOPF model is run with fixing the voltages at the generators' terminals. The voltages at the generators terminals are fixed at values obtained by the nonlinear ACOPF. We observe that in this case, the convex OPF is significantly accurate.

Figure 12 present the voltage profile on the 36-zone representative GB network with four different models. These models include the nonlinear ACOPF, the convex ACOPF, linear OPF started from the convex solution and linear OPF started from a cold start (i.e. all voltage magnitudes equal to 1 p.u. and all angle differences equal to zero). In this case, the voltage at generator terminals is not fixed because the generator transformers are collapsed at the zonal level. We observe that the convex OPF performs reasonably well and is able to predict the voltage profile with some errors. The ACOPF_LP model performs poorly for both initialisation point of the convex solution and the cold start. As noted earlier, the performance of the ACOPF_LP model is dependent on the initialisation point. This model is only useful when a solution is known and small changes are being made to a part of the network.

Table 3 presents the performance of the ACOPF and its approximations. We note that the convex formulation approximates the line losses with good accuracy, however, the flows in the network are slightly different as highlighted

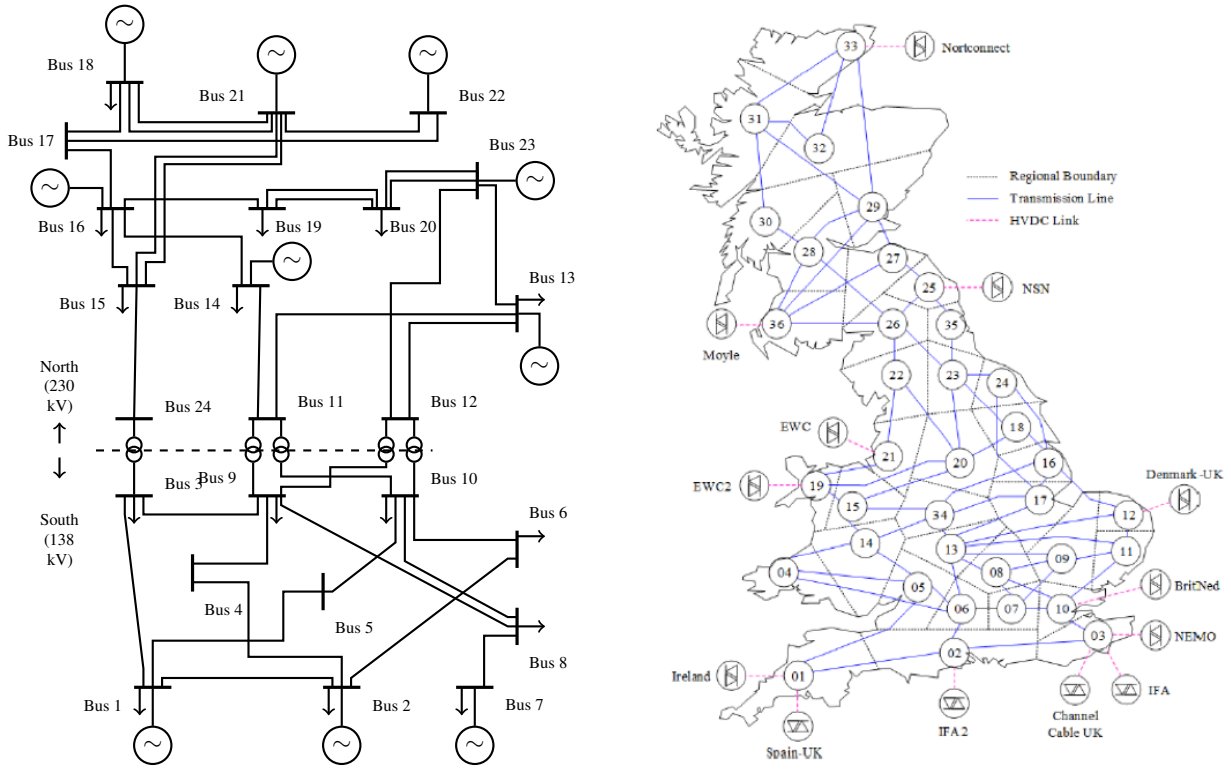

(a) Single line diagram of the IEEE 24-bus reliability test system [19].

(b) 36 zone GB representative network

Figure 10. Two test cases used for demonstration of the results.

by the root-mean squared error (RMSE) values. This is because the convex formulation is an approximation of the non-linear terms and it routes power in the network slightly differently than the ACOPF solution. The cold-start linear approximation performs poorly. As expected, the linear approximation using the ACOPF solution as a starting point is very accurate.

Figure 13 presents the voltage as a heat-map on the geographical map of the 36-zone GB network. For this network, the generators are modelled using the transformers so in total there are 132 buses. The demand in the network is increased by 40% at all buses and the convex OPF problem is solved on the model. Figure 13(a) presents the heat-map of voltages. We observe low voltages in zones 25 and 35 (zones indicated by an arrow). Figure 13(b) presents the results of the convex OPF with the commitment of a capacitor bank at zone 25. We note that the model decides to commit the capacitor bank because that results in improvement of the zonal transfers and results in reduced line loses. We also observe that the red colour which is indicative that the voltages are at their lower bound have disappeared following the commitment of the capacitor bank in Figure 13(b) in zones 25 and 35, respectively.

References

[1] Waqquas Bukhsh. NIA project code release 0.1, https://github.com/bukhsh/oats-nia, 3 2020.

[2] J. Carpentier. Contribution a l'etude du dispacting economique. *Bull. Soc. Francaise des Electriciens*, 3:431–447, 1962.

[3] Anya Castillo Mary B. Cain, Richard P. O Neill. History of optimal power flow and formulations. Technical report, Federal Energy Regulatory Commission, 2013.

[4] Richard P. O Neill Anya Castillo. Survey of approaches to solving the acopf. Technical report, Federal Energy Regulatory Commission, 2013.

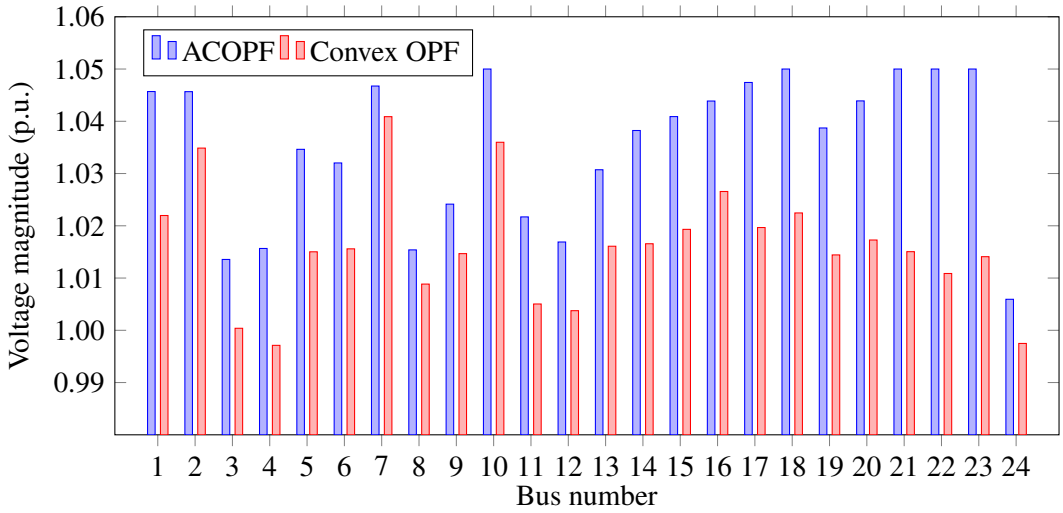

(a) Without fixing voltage magnitude.

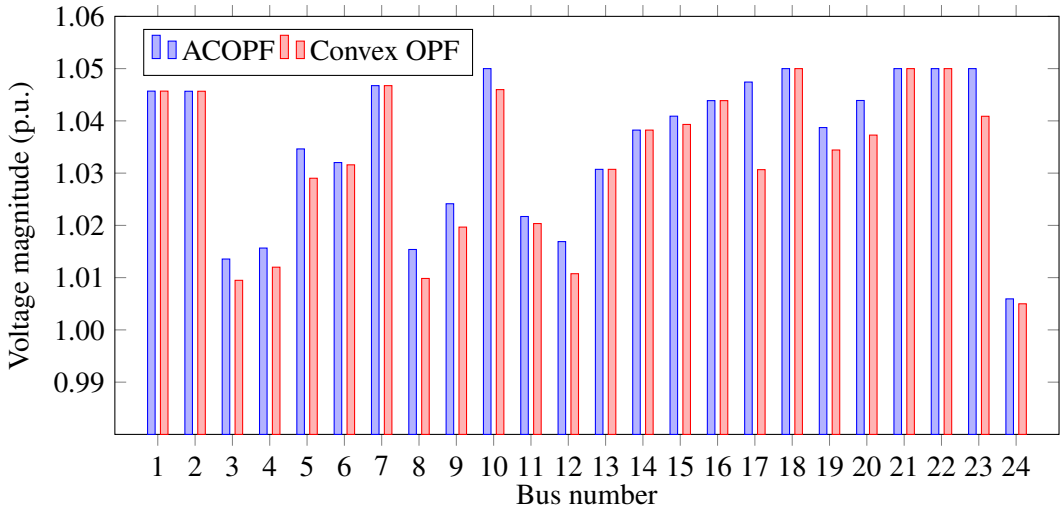

(b) Fixing voltage magnitude at the generator buses.

Figure 11. Comparison of solutions obtained by the nonlinear ACOPF and convex approximation with and without fixing voltage magnitude at the generator terminals.

[5] Richard P. O Neill Anya Castillo. Computational performance of solution techniques applied to the acopf. Technical report, Federal Energy Regulatory Commission, 2013.

[6] S. Cvijic, P. Feldmann, and M. Hie. Applications of homotopy for solving ac power flow and ac optimal power flow. In *Power and Energy Society General Meeting, 2012 IEEE*, pages 1–8, July 2012.

[7] Joseph Czyzyk, Michael P. Mesnier, and Jorge J. Moré. The neos server. *IEEE Journal on Computational Science and Engineering*, 5(3):68–75, 1998.

[8] Inc. Gurobi Optimization. Gurobi optimizer reference manual, 2016.

[9] A. Wächter and L. T. Biegler. On the implementation of an interior-point filter line-search algorithm for large-scale nonlinear programming. *Mathematical Programming*, 106:25–57, 2006.

[10] IBM ILOG CPLEX Optimizer. `http://www-01.ibm.com/software/integration/optimization/cplex-optimizer/`, Last 2010.

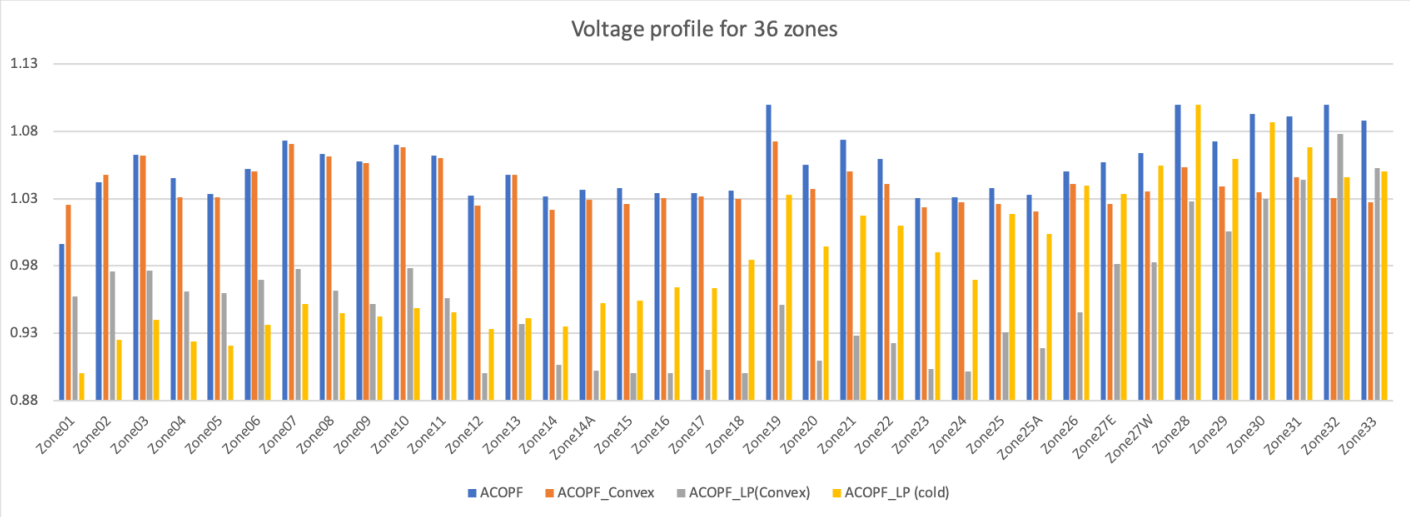

Figure 12. Voltage profile of the 36-zone network with four different models.

Table 3. Comparison of the approximation models with the solution of the nonlinear ACOPF problem when tested on the 36-zone representative GB test network. The approximation OPF_LP requires an initialisation: cold refers to a flat starting point, convex refers to the solution of the convex model and ACOPF refers to the solution of the nonlinear problem.

Model	Loss (%)	RMSE-Flows (MW)	RMSE-qG (MVar)
ACOPF	2.1	-	-
OPF_Convex	2.0	17.3	26.8
OPF_LP (cold)	0.2	73.2	210.3
OPF_LP (convex)	1.5	34.8	130.5
OPF_LP (ACOPF)	2.1	2.5	3.1

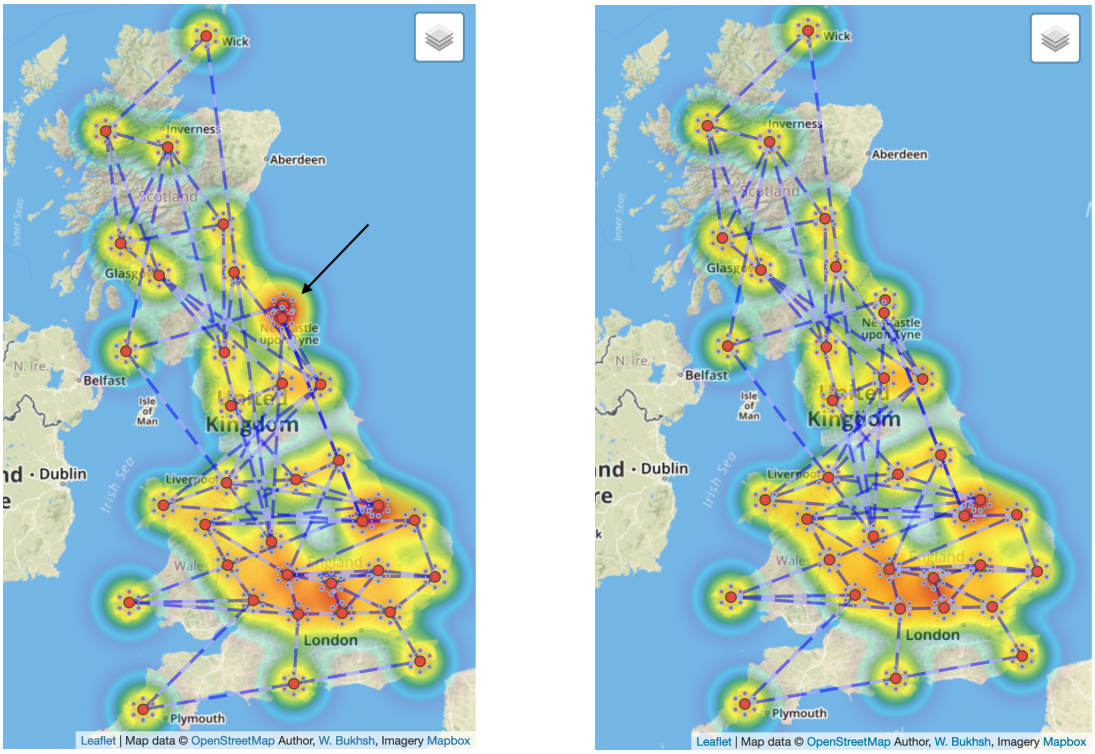

(a) Low voltages in two zones 25 and 35. These two zones are highlighted by an arrow.

(b) Low voltages improve by committing bank of capacitors in the zones 25 and 35.

Figure 13. Comparison of running an convex ACOPF problem with and without commitment of capacitor bank in zones 25 and 35.

[11] R. D. Zimmerman, C. E. Murillo-Sánchez, and R. J. Thomas. Matpower: Steady-state operations, planning, and analysis tools for power systems research and education. *IEEE Transactions on Power Systems*, 26:12–19, 2011.

[12] W.A. Bukhsh, A. Grothey, K.I.M. McKinnon, and P.A. Trodden. Local solutions of the optimal power flow problem. *Power Systems, IEEE Transactions on*, 28(4):4780–4788, 2013.

[13] National electricity transmission system security and quality of supply standard (netssqss), version 2.4. Technical report, 2018.

[14] Pascal V. Hentenryck Hassan L. Hijazi, Carleton Coffrin. Convex quadratic relaxations of nonlinear programs in power systems. *Optimization Online*, 2013.

[15] G. P. McCormick. Computability of global solutions to factorable nonconvex programs: Part 1-convex underestimating problems. *Mathematical Programming*, 10:146–175, 1976.

[16] H.P. Williams. *Model Building in Mathematical Programming*. Wiley, 2013.

[17] J. Y. Jackson. Interpretation and use of generator reactive capability diagrams. *IEEE Transactions on Industry and General Applications*, IGA-7(6):729–732, Nov 1971.

[18] H. Ambriz-Perez, E. Acha, and C. R. Fuerte-Esquivel. Advanced svc models for newton-raphson load flow and newton optimal power flow studies. *IEEE Transactions on Power Systems*, 15(1):129–136, Feb 2000.

[19] C. Grigg, P. Wong, P. Albrecht, R. Allan, M. Bhavaraju, R. Billinton, Q. Chen, C. Fong, S. Haddad, S. Kuruganty, W. Li, R. Mukerji, D. Patton, N. Rau, D. Reppen, A. Schneider, M. Shahidehpour, and C. Singh. The ieee reliability test system-1996. a report prepared by the reliability test system task force of the application of probability methods subcommittee. *IEEE Transactions on Power Systems*, 14(3):1010–1020, Aug 1999.